LANGMUIR Article
Cite This: Langmuir 2018, 34, 13395−13408
pubs.acs.org/Langmuir

Structural Characterization of Pluronic Micelles Swollen with Perfume Molecules

I. Grillo,*[,†] I. Morfin,[‡] and S. Prévost[†]

[†]Institut Laue Langevin, DS/LSS, CS 20156, 38042 Grenoble Cedex 9, France
[‡]Université Grenoble Alpes, LiPhy, 38000 Grenoble, France

Supporting Information

ABSTRACT: The insertion in nonionic polymer micelles (Pluronics F127) of seven essential oils and some of the pure compounds that compose them was investigated by complementary differential scanning calorimetry, small-angle X-ray, and neutron scattering (SAXS and SANS). The study revealed various insertion and swelling behaviors for the different oil molecules, an evidence of different interaction mechanisms involved between oils and Pluronic monomers. Thermodynamically, the addition of oil increased the micellization enthalpy due to an enhanced release of water molecules, leading subsequently to a decrease of the critical micellar temperature (CMT). Structurally, with oil, SANS revealed the presence of large aggregates at lower temperature than the CMT for which their size is maximal. Above the CMT, the size decreased and the equilibrium was reached a few degrees after the temperature corresponding to the maximum of the endothermic peak. At 37 °C, the detailed combined SANS and SAXS analysis demonstrated a partial phase separation between the oil and the poly(propylene oxide) core. The hydrophilic stabilizing poly(ethylene oxide) shell remains unchanged.

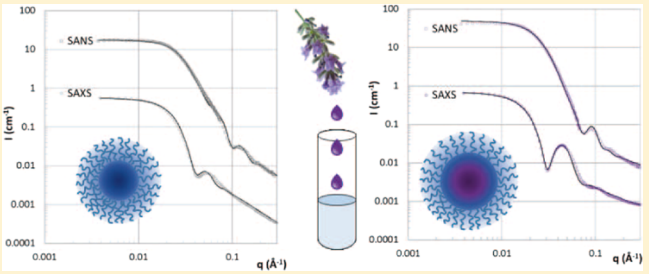

INTRODUCTION

Water solubilization and release of hydrophobic molecules is a key mechanism for pharmaceutical applications or cleaning processes. Increasing the water solubility of additives and active compounds is thus essential. This can be achieved using molecular mixture (cosolvency) or using solubility enhancers such as surfactants, forming containers able to encapsulate a hydrophobic molecule.[1,2] In the pharmaceutical domain, encapsulation plays an important role to protect from oxidation and to maintain the biological activity of active compounds.[3] For cosmetic products, it helps in controlling volatility and release properties,[4,5] whereas in food industry, it limits the degradation in composition during processing and storage. Depollution and water waste treatment also benefit from the solubilization capability of surfactant aggregates, to allow a local enrichment of a given compound for separation from a dilute solution. In the presence of micelle-forming amphiphiles, additives may see their water solubility increase due to cosolvency with a change in chemical potential,[6] or due to loading inside the micelles, at various locations, more or less deep inside the structure.[7]

However, it is largely recognized that the incorporation of hydrophobic molecules has a significant influence on the surfactant assemblies according to their location from the inner core to the solvated corona, via the core/shell region. It can induce drastic growth of micelles, phase transition, and separation.[8−10] The exact localization of incorporated molecules in surfactant aggregates is thus crucial to understand the release dynamics and the interactions, which further determine the product properties such as stability and shelf-life, two major issues in industrial applications.[11] In addition, more specifically for pharmaceutical applications, the structural changes that promote the aggregate growth can affect seriously the properties and usability of the drug nanocarriers if some critical size is exceeded. A detailed knowledge of the impact of additives on the nanocarrier primary structure is mandatory and can help optimize the design and efficiency.

In this study, essential oils are chosen as a representative class of hydrophobic but slightly polar molecules. They are known and used since ancient times for their fragrance and medicinal properties. Their effects in pharmaceutical preparations are described in official pharmacopeias and belong to the traditional medicine. Essential oils are extracted from plants and are complex blends of a variety of volatile molecules such as hydrocarbons (terpenes) and oxygenated molecules (alcohols, esters, ethers, aldehydes, ketones, lactones, phenols, and phenol ethers). Ethylene oxides (EOs) can contain up to 60 different components with one to three compounds at high concentrations (20−70%) and the others present in trace amounts. The main compounds determine the biological and medicinal properties, such as antibacterial, virucidal, fungicidal, insecticidal, analgesic, anti-inflammatory, or anesthetic. A large scientific literature domain is dedicated to the use of these natural products for maintaining health and potentially treating

Received: September 7, 2018
Revised: October 10, 2018
Published: October 12, 2018

Downloaded via INST LAUE-LANGEVIN on May 3, 2019 at 09:31:12 (UTC).
See https://pubs.acs.org/sharingguidelines for options on how to legitimately share published articles.

© 2018 American Chemical Society

DOI: 10.1021/acs.langmuir.8b03050
Langmuir 2018, 34, 13395−13408

Table 1. Molecular Structure of the Perfume Molecules (a) Anethol, (b) Thymol, (c) Limonene, (d) 1-8 Cineol (Eucalyptol), (e) Linalool, (f) Geraniol, (g) 4-Terpineol, (h) Menthol, and (i) Methyl Salicylate

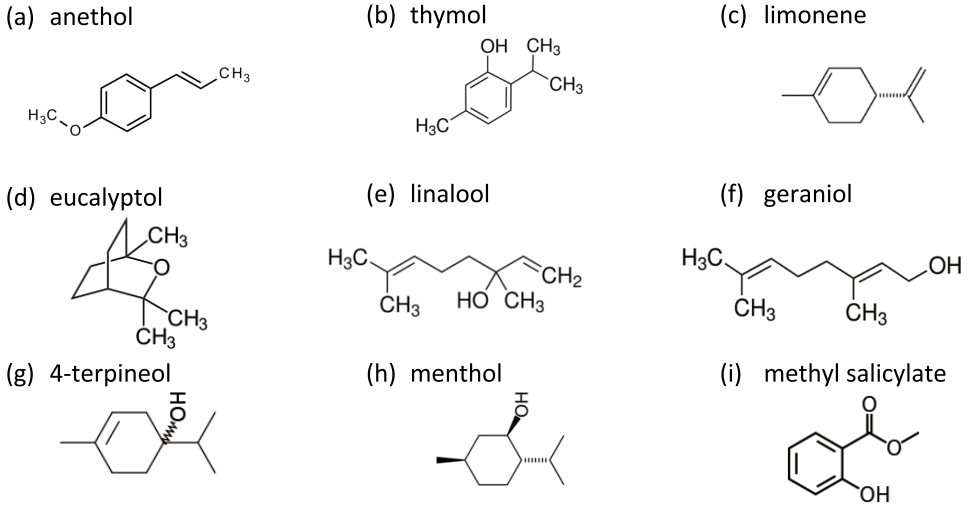

diseases.[12,13] Essential oils or rather the synthesized perfume molecules are also widely found in commercial, cosmetic, home care, and food and drink products to improve taste or flavor. Essential oils are hydrophobic and thus almost not soluble in water, which obliges dissolving them in an organic solvent. For water-based formulations used in cosmetics, food products, and pharmaceutical formulations, these hydrophobic active molecules are encapsulated into amphiphilic carriers such as micelles or vesicles that enhance the water solubility and oxidative stability and decrease the volatility and slow down the release.[4,5,14]

The oil molecules can be classified according to their water solubility or their partition coefficient log(P), which quantifies the ratio of the concentrations of the oil in octanol and water at equilibrium and thus their relative hydrophilicity/hydrophobicity. Several studies tend to demonstrate a link between log(P) and the location within the micelles. In ref 15, a comprehensive study on the incorporation of 20 fragrance molecules in mixed anionic−nonionic micelles shows three distinct behaviors according to the log(P) value. Hydrophilic fragrances (log(P) < 2) are distributed almost equally between the micellar and aqueous phases. Hydrophobic fragrances (log(P) > 3.5) are fully solubilized in the micelles. The situation is more complex in the intermediate log(P) region where a strong dependence of fragrance partitioning on the chemical structure superimposes the general dependence on hydrophobicity. Bulky structures, such as alcohols with a long and partly branched chain (methyl groups or rings), are extremely hindered in their isotropic motions and remain at the interface, whereas compounds with long alkyl chains are incorporated to a higher degree in the micelle core. Other studies corroborate this insertion behavior in micelles of small-molecular-weight surfactants.[16,17]

Pluronics (Poloxamers) are a wide family of triblock copolymers composed of two hydrophilic poly(ethylene oxide) (PEO) groups and a central hydrophobic poly(propylene oxide) (PPO) group with the general chemical formula $HO[CH_2CH_2O]x[CH(CH_3)CH_2O]y[CH_2CH_2O]xOH$. The self-assembling properties, the size, and the nature of so-formed aggregates are easily varied by changing the PEO/PPO ratio. They are largely studied for encapsulation and drug delivery because they present low critical micellar concentrations (CMC), critical micellization temperatures (CMT) between 20 and 40 °C, below or close to the body temperature, and form micelles of diameter from 200 to 800 Å, which is the most appropriate size range for drug delivery. In addition, the presence of flexible and uncharged PEO chains with a high steric hindrance enhances the circulation time in the bloodstream.[18] In the large Pluronic family, F127 (EO_{100}-PO_{65}-EO_{100}) possesses thermoreversible and rheological properties that are of the greatest interest in enhancing drug formulations.[19]

Since Pluronics show high potential as nanocarrier, broad literature is found on the incorporation of hydrophobic molecules in Pluronic aggregates. Small-angle neutron scattering (SANS) with the possibility of specific deuteration has been widely used to characterize the structure of these multicompartment systems, and complementary nuclear Overhauser effect spectroscopy (NOESY) experiments allowed to identify the locus of solubilization.[20−29] These experimental results can be further compared to the predictive thermodynamic model developed by Nagarajan et al.[30−34] where the solubilization capacity of hydrocarbon in Pluronics and the effects on the micellar size and shape are calculated. However, general rules that govern the loading capability correlated with the location of the oil within the micelle are still unclear and still little is known concerning the structure of Pluronic micelles with EOs.

In the following discussion, we investigated the insertion in the Pluronic F127 micelles of seven EOs, lemon, rosemary, lavender, palmarosa, tea tree, mint, and gaultheria and nine main perfume molecules that compose them, limonene, anethol, thymol, eucalyptol, linalool, geraniol, terpineol, menthol, and methyl salicylate. The choice of these EOs/molecules was driven by their widespread use as perfume or flavor in industrial products (lemon, lavender/linalool, palmarosa/geraniol, and mint/menthol) and for their therapeutic properties, such as antibacterial, fungicidal, antiseptic (thymol and tea tree/terpineol),[35,36] anti-inflammatory (gaultheria/methyl salicylate), and cough suppressant property, and as insect repellent (rosemary/eucalyptol)[37,38] and local anesthetic (mint/menthol).[39] They also illustrate the

DOI: 10.1021/acs.langmuir.8b03050
Langmuir 2018, 34, 13395−13408

Table 2. List of the Essential Oils with Their Main Molecules, Chemical Formulas, Molecular Weight, Densities, Solubility in Water/Octanol Partition, and Neutron and X-ray Scattering Length Densities (ρ)[a]

molecule/EO	formula	molar mass	volumetric mass density (g/mL)	solubility (g/L)	log(P)	ρ (neutron) (cm^{-2})	ρ (X-ray) (cm^{-2})
anethol star/anise	$C_{10}H_{12}O$	148.21	0.98	0.111	2.43[b]	1.11×10^{10}	9.17×10^{10}
thymol/thyme	$C_{10}H_{14}O$	150.22	0.965	0.9	3.3[c]	0.767×10^{10}	8.92×10^{10}
limonene/lemon	$C_{10}H_{16}$	136.23	0.84	0.014	4.38[b]	0.246×10^{10}	7.97×10^{10}
1-8 cineol or eucalyptol/rosemary	$C_{10}H_{18}O$	154.25	0.921	3	2.74[c]	0.178×10^{10}	8.73×10^{10}
linalool/lavender	$C_{10}H_{18}O$	154.25	0.858	1.6	2.44[b]	0.166×10^{10}	8.14×10^{10}
geraniol/palmarosa	$C_{10}H_{18}O$	154.25	0.879	0.1	3.56[c]	0.172×10^{10}	8.44×10^{10}
4-terpineol/tea tree	$C_{10}H_{18}O$	154.25	0.93	0.38	3.2[c]	0.18×10^{10}	8.85×10^{10}
menthol/mint	$C_{10}H_{20}O$	156.27	0.89	0.45	3.06[b]	-0.881×10^{10}	8.65×10^{10}
methyl salicylate/gaultheria	$C_8H_8O_3$	152.15	1.17	0.7	2.08[b]	1.9×10^{10}	10.6×10^{10}

[a]The solubility values were taken from https://pubchem.ncbi.nlm.nih.gov/. [b]Value reported from ref 16. [c]https://pubchem.ncbi.nlm.nih.gov/.

variety of chemical natures, such as polarity, water solubility, and structure of the perfume molecules (see Table 1).

We worked in the dilute part of the F127 phase diagram where micelles are formed in water.[40] Differential scanning calorimetry (DSC) was used to determine the effect of the different additives on the critical micellar temperature (CMT). The detailed characterization of the micelles was obtained by a combined use of small-angle X-ray and neutron scattering (SAXS and SANS).[41] SANS is mostly sensitive to the hydrophobic core, and the hydrophilic shell being almost invisible due to its high hydration has only a small contribution. SAXS give a full description of the micelles, and the high flux and resolution of synchrotron instruments allow for resolving the form factor oscillations, whose position and amplitude are closely linked to the partition of the oil into the micelle. The complementarity of the two techniques is due to the significantly different scattering length density (SLD) for X-rays (sensitive to electronic density, usually EO > propylene oxide (PO) > water > essential oil) and neutrons (primarily sensitive to the H/D isotopic composition, with typically deuterated solvent ≫ EO > PO > essential oil). The subtle changes of SLD profiles upon incorporation of oil affect in a different manner the SANS and SAXS scattering curves, as it will be shown in the experimental part and associated figures, and allow one to locate the position of the oil in the micelle.

MATERIAL AND METHODS

Chemicals. D_2O (99.9%), Pluronic F127, and the synthetic perfume molecules, anethol, limonene, linalool, geraniol, eucalyptol, menthol, thymol, methyl salicylate, and terpineol, were purchased from Aldrich and used without further purification. The essential oils issued from organic farming, lavender (Lavandula angustifolia), palmarosa, gaultheria, lemon, eucalyptol, peppermint, and tea tree, were bought in specialized shops. The structure of the different perfume molecules is presented in Table 1. Their physical parameters, molar mass, density, solubility in water, log(P), and neutron and X-ray SLD are summarized in Table 2. Apart from lemon (limonene), all molecules have log(P) between 2 and 4, i.e., in the intermediate domains.[16] These oils are also broadly used in industrial fields. Except for the methyl salicylate, the neutron and X-ray SLD of the oils is lower than the polymer SLD. The incorporation of these molecules in the Pluronic micelles, in addition to a swelling, modifies the contrast between the hydrophilic and hydrophobic parts and thus the scattering profile.

The samples were all prepared in D_2O to increase the scattering length density contrast and to reduce the incoherent background for SANS experiments. The samples were characterized by the volume fraction of F127 Φ_{F127} in D_2O and the total volume fraction of Φ_{oil}.

$$\Phi_{F127} = \frac{V_{F127}}{V_{F127} + V_{D_2O} + V_{oil}} \text{ and } \Phi_{oil} = \frac{V_{oil}}{V_{F127} + V_{D_2O} + V_{oil}}$$

A stock solution of F127 in D_2O at Φ_{F127} = 1% was prepared by weighting out the appropriated amounts of F127 and solvent and gently stirred for 1 day. The solution was then kept at laboratory temperature (20 °C). The appropriate amount of oil was weighed out and added to the F127 stock solution to obtain the requested oil volume fraction Φ_{oil}. The samples were vortexed and left for equilibration in the dark at least for 2 days before further analysis. For menthol and thymol that are powders at room temperature, the samples were heated to 40 °C and sonicated until complete dissolution.

To determine the insertion limit, the oil concentration was progressively increased by 0.02 vol % steps, defining the error on the concentration limit. After equilibration, the samples were visually inspected and the presence of tiny droplets in solution after gentle shaking indicated a phase separation. For thymol, a different behavior was observed with the appearance of an opalescent but homogenous phase.

Differential Scanning Calorimetry (DSC). Differential scanning calorimetry measurement was carried out with a Micro DSC III apparatus (Setaram, France) that allows high sensitivity with dilute solutions. The sample of about 0.4 g was placed in a Hastelloy vessel and the same amount of D_2O was used as reference. A first fast cycle at 2 K/min between 4 and 60 °C was performed to ensure the homogeneity of the solution. Then, two cycles at 0.5 K/min were repeated to check reproducibility and reversibility of the transition. The CMT was determined from the temperature at the intersection of the tangent of the first inflection point of the peak with the baseline.[42] The enthalpy of micellization (ΔH_m) was calculated from the area of the micellization peak.

Drop Shape Analysis. The interfacial tension between the oil and the water was measured at room temperature using a drop-shaped analyzer DSA10 from Krüss. For molecules with densities lower than 1, drops of oil in heavy water were created using an inverted blunt needle of 0.72 mm outer diameter immersed in a 10 mm × 20 mm × 40 mm optical glass cuvette. For methyl salicylate, a pendant drop was created using a flat needle of 0.7 mm diameter. Interfacial tensions were calculated from the drop-shaped profiles by the Krüss software using the Young−Laplace equation.

Zetasizer. The hydrodynamic radii of the loaded micelles at the maximal insertion were determined by dynamic light scattering (DLS) method (Zetasizer Nano ZS; Malvern Instruments, U.K.) and at a scattering angle of 90°. The temperature was set at 37 °C. The samples were filtered (Millex GV poly(vinylidene fluoride) hydrophilic, 0.22 μm) and analyzed without dilution.

Small-Angle Neutron Scattering (SANS). The SANS experiments were performed on the D22 and D33 instruments at the Institut Laue-Langevin (Grenoble, France). Two instrument configurations were used to cover a q-range from 3×10^{-3} to 0.4 $Å^{-1}$ where the scattering vector q is defined as $q = 4\pi/\lambda \sin\theta$, 2θ being the

DOI: 10.1021/acs.langmuir.8b03050
Langmuir 2018, 34, 13395−13408

scattering angle and λ the neutron wavelength. On D22: λ = 6 Å, sample-to-detector distance D = 2 m, collimation C = 5.6 m, and D = 14 m, C = 14.4 m, and detector offset = 300 mm; on D33, λ = 6 Å, D = 2 m, C = 7.8 m and D = 12 m, C = 12.8 m. The long collimation distance compared with the detector distance at the high q configuration allows for a good resolution in q. The samples were placed in 1 mm path length Hellma cells and thermostated using a circulating water bath. The raw scattering data were corrected for the electronic background and empty cell and were normalized on the absolute scale using the attenuated direct beam to calculate the incident flux, using ILL Lamp software (https://www.ill.eu/instruments-support/computing-for-science/cs-software/all-software/lamp/).

Small-Angle X-ray Scattering (SAXS). SAXS measurements were performed at the high-brilliance beamline ID02 at the ESRF (Grenoble, France), in four-bunch mode and with a 1 mm graphite attenuator, to prevent radiation damage. A energy of 12.46 keV (λ = 0.0995 nm, relative full width at half-maximum 10^{-4}) was used. The Rayonix MX-170HS charge-coupled device detector in 8 × 8 binning was set at a sample-to-detector distance of 2 m, as verified with silver behenate calibration standard. Samples were inserted into a Peltier-thermalized flow-through quartz capillary of 2 mm inner diameter measured by transmission scan. Data were corrected for the dark current, flat field, incoming flux, and transmitted beam measured simultaneously with scattering. Ten measurements were averaged after verifying that no change due to radiation damage occurred. Contribution of the solvent (D_2O)-filled capillary was subtracted. The absolute scale was determined using the plateau intensity level of water (at 1.63 × 10^{-2} cm^{-1} at 298 K).

SANS and SAXS Data Analysis. The detailed equations of the form and structure factors used for the SANS and SAXS data analysis are given in the Supporting Information. The scattering of the pure Pluronic micelles is fitted to a core−shell model combined with a hard-sphere (HS) structure factor. The core contains PPO and water, and the shell contains PEO and water. The resulting parameters are R_0 the core radius, e_{shell} the thickness of the PEO shell, the core and shell SLD, and Φ_{HS_m} the hard-sphere volume fraction of micelles. A Gaussian coil with R_g = 6 Å is added to improve the fitting at high q (> 0.2 $Å^{-1}$), which originates from the PEO segment. Polydispersity (with a Gaussian distribution of sizes) is applied to the core and the shells independently. Finally, the instrument resolution with appropriate weight function is taken into account in the fitting procedure.

In presence of the oil molecules, assuming that the oil deeply penetrates into the micellar core, a core−two-shell model combined with HS structure factor is used. According to the nature of the oil and its location in the micelle, the multilevel structure composition can vary: the core might contain, in various amounts, oil and PPO, the first shell might contain oil, PPO, and water and the second shell might contain oil, PEO and water.

The resulting parameters are the radius of the enriched oily core R_0, the thickness of the PPO layer e_{PPO}, the PEO shell thickness e_{shell}, the scattering length densities of the different layers, and the volume fraction of micelles Φ_m that is also used for calculation of the hard-sphere structure factor. From these parameters, we can extract the solvent hydration in the different shells, the density number of micelles and their aggregation number, and the surface per head group. The analysis is done using SasView 3.1.2 software package (http://www.sasview.org/).

The shell of the Pluronic micelles is highly hydrated, and the average scattering length density $\bar{\rho}_{PEO}$ is equal to

$$\bar{\rho}_{shell} = f_{shell}\rho_{D_2O} + (1 - f_{shell})\rho_{EO} \quad (1)$$

with f_{shell} the volume fraction of D_2O in the shell. ρ_{D2O} and ρ_{EO} are the SLD of D_2O and EO, respectively.

The PPO core is to a less extent hydrated.[43] The average core SLD is then equal to

$$\bar{\rho}_{core} = f_{core}\rho_{D_2O} + (1 - f_{core})\rho_{PO} \quad (2)$$

with f_{core} the volume fraction of D_2O. ρ_{PO} is the SLD of PO calculated taking account the apparent specific molecular volume of PO in the micellar state, as determined in ref 44.

In presence of oil, the calculation of the scattering length densities in the different compartments of the micelles is delicate. This implies the knowledge of the volume fractions of PO, oil, EO, and D_2O in each part. These different ratios, however, depend on the added oil molecule, and the combined SANS and SAXS experiments do not allow for solving such equations without further assumptions.

With R_{tot} equal to R_0 + e_{PPO} + e_{shell}, the total volume of one hydrated micelle is

$$v_m = 4/3\pi {R_{tot}}^3 \quad (3)$$

The density number of particles per cm^3 N_p is obtained by dividing the volume fraction of micelles Φ_{HS_m} by the micellar volume v_m

$$N_p = \Phi_{HS_m}/v_m \quad (4)$$

The aggregation number is calculated by dividing the volume fraction of F127 known from the sample preparation (1%) by the density number of micelles and the molecular volume of one F127 molecule

$$N_{agg} = \frac{\Phi_{F127}}{N_p v_m^{F127}} \quad (5)$$

Finally, by considering a hairpin configuration of the Pluronic chain and one head group per molecule, the surface per head group at the interface between the PEO and PPO shell is obtained as follows

$$\sigma = \frac{4\pi(R_o + e_{PPO})^2}{N_{agg}} \quad (6)$$

EXPERIMENTAL RESULTS

Oil Insertion Limit in Pluronics F127. Figure S1 (Supporting Information) shows the total maximal volume fraction of oil Φ_{oil}^L that enters in a 1% solution of F127 before the apparition of oil droplets and these limits are compared to the oil−water solubility.

We observe that the most water-soluble oils, thymol, eucalyptol, and linalool have the highest limits, but that is mainly due to the fact that a part of the oil remains in the water. The important information is about the volume of oil that is really encapsulated into the micelles. In the first approximation, we consider that the water solubility of the oils is not modified by the presence of Pluronic molecules. Then, the insertion limit S_{oil}^L is defined as

$$S_{oil}^L = (\Phi_{oil}^L - (S_{oil}/d_{oil})/1000)/\Phi_{F127} \quad (7)$$

S_{oil} and d_{oil} are the oil−water solubility in g/L and density, respectively. Φ_{oil}^L is the total maximal volume fraction of oil determined experimentally and Φ_{F127} is the volume fraction of F127.

The insertion limits for the different oil molecules are shown in Figure 1 (left axis). These limits are compared to the hydrodynamic radius measured by DLS (Figure 1, right axis). After correction from the oil dissolved in water (eq 7), the insertion limit still depends strongly on the oil molecule. 4-Terpineol shows the highest encapsulation limit (0.41), followed by thymol and linalool, close to 0.3. Limonene has the smallest solubility in the micelles (0.08). The other molecules have limits of around 0.15. DLS measurements show a significant increase of the hydrodynamic radius of the micelles in presence of the oil, compare R_h = 142 Å for F127 in D_2O confirming the incorporation of the oil into the micelles. We notice also that the hydrodynamic radius is not proportional to the solubility limit; such behavior can only be explained by different localizations of the oil molecules into the micelle.

In the following, we are working at a concentration of 1% for the F127 and an oil volume fraction of 0.2% to remain in the monophasic domain for the majority of the oils (except limonene and methyl salicylate). This volume corresponds to 20 vol % of the (dry) Pluronic volume, 60% of the PPO volume, and 40 oil molecules per PPO moiety or 0.6 oil molecule per PO group. In such conditions, at 37

DOI: 10.1021/acs.langmuir.8b03050
Langmuir 2018, 34, 13395−13408

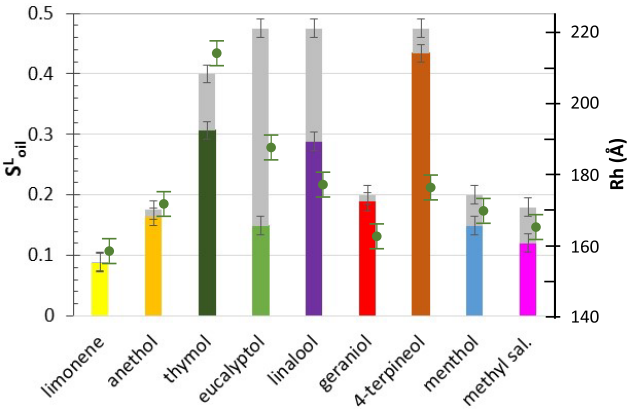

Figure 1. (Bar, left axis) Insertion limit of the oil molecules in 1% F127 at 37 °C. Gray bars correspond to the total oil volume fraction before phase separation. Color bars are the oil volume fraction in the micelles after subtraction of the remaining oil in water (eq 7) (●, right axis). Hydrodynamic radius measured by DLS at the insertion limit. R_h = 142 Å for F127 in D_2O.

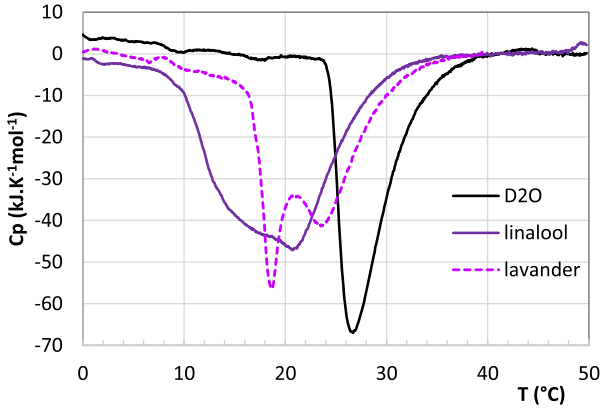

Figure 2. DSC thermograms showing the effect of 0.2% of linalool or lavender on the micellization process of 1% F127 solution.

°C, all samples were transparent except those containing limonene or lemon in which tiny droplets were visible by eyes (Table 3).

DSC Measurements. Figure 2 presents the thermograms for linalool and lavender in 1% F127 solution in comparison with the "pure" micelles in D_2O. The thermograms for the different synthetic molecules or essential oils are compared in Figure 3. Table 4 summarizes the CMTs and micellization enthalpies.

The pronounced endothermic peak is a signature of the micellar formation induced by the dehydration of the PPO. For the reference solution, the temperature onset (CMT) is found at 24 °C, in good agreement with the literature.[40,45] Except for thymol for which the peak disappears, the endothermic peak is always present with the oils. Its position is shifted to a lower temperature that depends on the additive. The lowest CMTs around 11 °C are obtained for geraniol and linalool. We can notice that these two molecules do not possess aromatic rings. The other molecules have less impact, and the onset of micellization occurs around 19 °C. The peak becomes also larger, and a split is observed for geraniol, menthol, and all essential oils except gaultheria (methyl salicylate) and lemon (limonene).

Pluronics are diblock terpolymers with distributed block lengths, leading to a distribution in amphiphilicity and thus in hydrophobicity of the Pluronic molecules. The most hydrophobic molecules become dehydrated at lower temperatures and begin the micellization. At higher temperatures, redistribution and homogenization of the oil in the micelle occur.[16] However, as the split is mostly observed with the EOs rather than with the synthetic molecules, the origin might also be due to the various compounds making up the blend, that induce different micellization temperatures. In such a case, it may indicate that Pluronic F127 micelles are able to separate different hydrophobic molecules in these complex mixtures.

The micellization entropy of the 1% F127 solution is 357 kJ/mol, in good agreement with the literature.[46] The presence of oil induces a significant increase of the enthalpy. The strongest effects are found for linalool and menthol. Such increase in enthalpy is linked to the release of water molecules: the solvation water is displaced by the incorporation of oil. This has already been reported for F108 and P84 Pluronic molecules in presence of different oils[25,47] and with P123 with long-chain alcohol, confirmed by NMR.[48] A cooperative association of the alkanol chains with the PO groups expels the water and favors the micellization.

SANS Investigation of the Micellization Process as a Function of Temperature. The DSC experiments have shown that the addition of the perfume molecules promotes the micellization that starts at lower temperatures. Here, we aim to follow by SANS the formation and disruption of the micelles during the heating and cooling phases. The sample F127 1% in D_2O is taken as reference and six molecules, anethol, thymol, linalool, geraniol, eucalyptol, and methyl salicylate, characteristic of the diversity of the oils, are investigated. The temperature is increased from 8 to 37 °C and then cooled down to 8 °C to check for the reversibility. At each step, at least 10 min are left for temperature equilibration.

The data for the F127 in D_2O are presented in the Supporting Information (Figure SI2). Below the CMT determined at 24 °C by DSC, water is a good solvent for both the PPO and PEO blocks and the F127 is in the form of monomers. The curves are almost superimposed, except for a small increase of the intensity at low-q with increasing T. The radius of gyration of the chains obtained with the Guinier–Debye model is 40 Å, in good agreement with a previous scattering study.[49] At 24 °C, the scattering pattern still corresponds to that of a polymer chain at high q but a significant increase of the forward scattering is obtained and the radius of gyration increases to 75 Å. At 29 °C, the transition has occurred and the typical signal of micelles is visible. The data analysis following a core–shell model gives a core of 42 Å and a shell of 61 Å. From 29 to 37 °C, the scattering intensity still increases at low q and the data fitting shows a small increase of the core radius up to its final size at 45 Å.

In presence of oil, one observes a different behavior. An example is shown in Figure 4 for linalool. The results with the other oils are

Table 3. F127 and Solvent Chemical Data: Chemical Formulas, Molecular Weights, Densities, and Neutron and X-ray Scattering Length Densities at 37 °C[a]

	formula	molar mass (g/mol)	volumetric mass density (g/mL)	molecular volume (Å^3)	ρ (neutron) (cm^{-2})	ρ (X-ray) (cm^{-2})
F127 (EO)100(PO)65(EO)100		12 570	1.128	18 503		
(PO)	($OCH(CH_3)CH_2$)	58	1.024	94	0.34×10^{10}	9.58×10^{10}
(EO)	(C_2H_4O)	44	1.18	62	0.67×10^{10}	10.9×10^{10}
solvent	D_2O	20	1.1045	30.1	6.36×10^{10}	9.38×10^{10}

[a]The PO and PEO density values are taken as determined in 44.

DOI: 10.1021/acs.langmuir.8b03050
Langmuir 2018, 34, 13395−13408

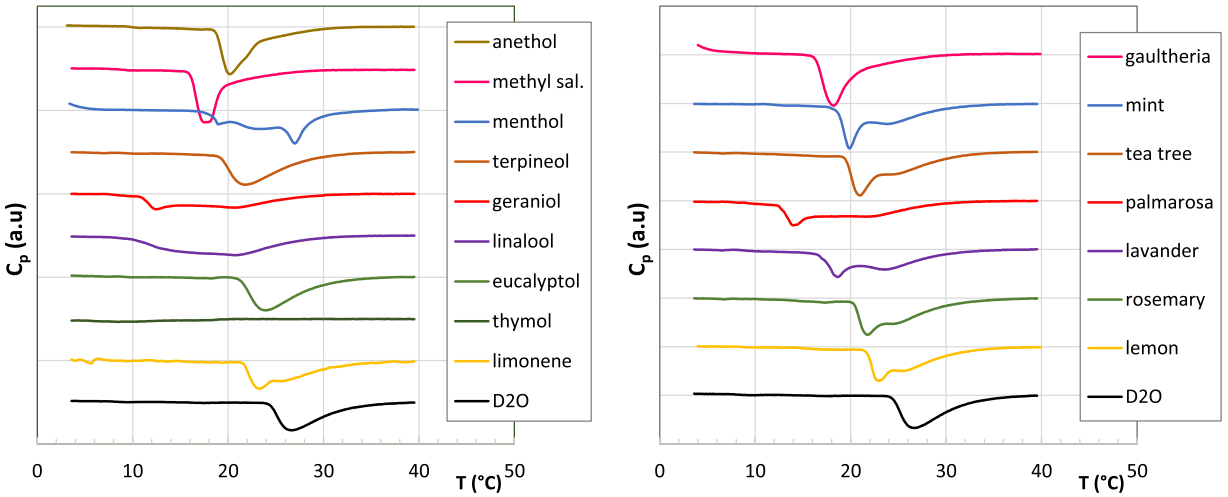

Figure 3. DSC thermograms for 1% F127 solution with 0.2% of oil. Comparison between the synthetic molecules (a) and the essential oils (b). The curves are shifted for clarity reason.

Table 4. Thermodynamic Parameters of the Micellization Process for Solutions F127 1% with 0.2% Oil: CMT, Temperature at the Peak Maximum, and Enthalpy

molecule	CMT (°C)	T_{max} (°C)	ΔH_m (kJ/mol)
D_2O	24.6	26.7	357
limonene	21.8	23.2	365
anethol	18.8	20.3	412
thymol	<0	<0	
eucalyptol	21.5	23.9	470
linalool	11.5	20.7	557
geraniol	11.0	12.6	434
terpineol	19.4	21.9	484
menthol	18.2	27.0	502
methyl sal.	16.2	17.5	428
EO	CMT (°C)	T_{max} (°C)	ΔH_m (kJ/mol)
D_2O	24.6	26.7	357
lemon	21.8	23.0	342
rosemary	20.3	21.7	385
lavender	17.2	18.6	406
palmarosa	12.6	14.0	464
tea tree	18.6	21.0	405
mint	18.7	19.9	408
gaultheria	16.4	18.3	437

presented in the Supporting Information (Figures S3–S9). At 8 °C, the scattering curve is very similar to a polymer coil but the gyration radius of 80 Å obtained from the analysis is too large for the F127 monomer. The scattering is rather the sum of F127 monomers in coexistence with a few larger objects. The curve is thus fitted with the sum of a core–shell spherical model and polymer Gaussian chains. At this step, the particles have a core of 100 Å. The shell thickness is fixed at 61 Å. Their volume fraction is very low, around 0.002%, and they are in equilibrium with free polymeric chains with an R_g of 40 Å. At 10 °C, just at the temperature onset of the CMT, the presence of large aggregate is confirmed; their volume fraction has increased (around 0.05%), and the core reaches a maximum size of 125 Å. By increasing the temperature, the core radius decreases down to 64 Å at 22 °C, the temperature corresponding to the maximum of the endothermic peak, and then remains stable. The micelle volume fraction is at this point 2.4% and increases up to 3.4% when the equilibrium in size is reached at 29 °C. The latter value coincides with the end of the endothermic transition. From 29 to 37 °C, the volume fraction of micelles continues to increase up to 4.7%. During the entire process, the shell thickness is fixed at 61 Å.

By lowering the temperature from 37 down to 8 °C, a decrease in size of the hydrophobic core from 62 to 54 Å at 17 °C is observed. From 17 down to 11 °C, the aggregates grow again in size but they are smaller than the size of the aggregates formed at the same temperature during the heating phase. Finally, at 8 °C, the curves measured during the heating or cooling are superimposed. Figure 5 summarizes the evolution of the size of the hydrophobic core during the heating and cooling phase and clearly evidences a hysteresis process.

For thymol, the micelles are already formed in their final state at 8 °C, in agreement with the absence of the endothermic peak characteristic from the micellization in the temperature range investigated. For the other molecules, the mechanism observed with linalool can be generalized (Figure S10). With anethol and eucalyptol (Figures S4 and 6), since the CMT remains relatively high, the first temperature is well below the CMT and the scattering is mainly dominated by the scattering of the polymer chain. However, contrary to the pure F127 in D_2O, the scattering curve cannot be modeled by a Gaussian coil, due to the increase of the scattering intensity at small q values. Getting closer to the CMT, for all molecules, an oscillation appears, corresponding to aggregates with a size of more than 100 Å that were not visible without oil. Their volume fraction remains, however, low. The oscillation becomes more pronounced as the temperature increases, and the size of the aggregates increases strongly up to the onset of the CMT. From this temperature and up to T_{peak}, the size decreases and the volume fraction increases. The equilibrium in size and volume fraction is attained a few degrees after T_{peak}. During the cooling phase from 37 to ca. 17 °C, a deswelling of a few angstroms is first observed followed by a reswelling of around 20 Å. The micelle size remains anyway much smaller than that measured at the same temperature during the heating phase. Finally, at the lowest temperature of 8 °C, the scattering curves are superimposed with the initial measurements. The observed hysteresis suggests the existence of slow relaxation time during the micellization/dissolution process, as introduced and described by Aniansson and Wall,[50] and further confirms the impact of additive on the stability and dynamics of the micelles.[51]

Detailed Combined SANS and SAXS Structural Characterization of the Micelles at 37 °C. *Pure F127 Micelles.* The full understanding of the structure of the oil-loaded micelles is only possible once the structural conformation of the micelles is correctly described, which implies the full consistency between SANS and SAXS parameters with respect to the composition.

The SANS and SAXS scattering data analysis of a 1% F127 solution in D_2O at 37 °C with the scattering length density profiles is presented in Figure S11 in the Supporting Information. In Figure S12, the different contributions from the core–shell and Gaussian coils are

DOI: 10.1021/acs.langmuir.8b03050
Langmuir 2018, 34, 13395–13408

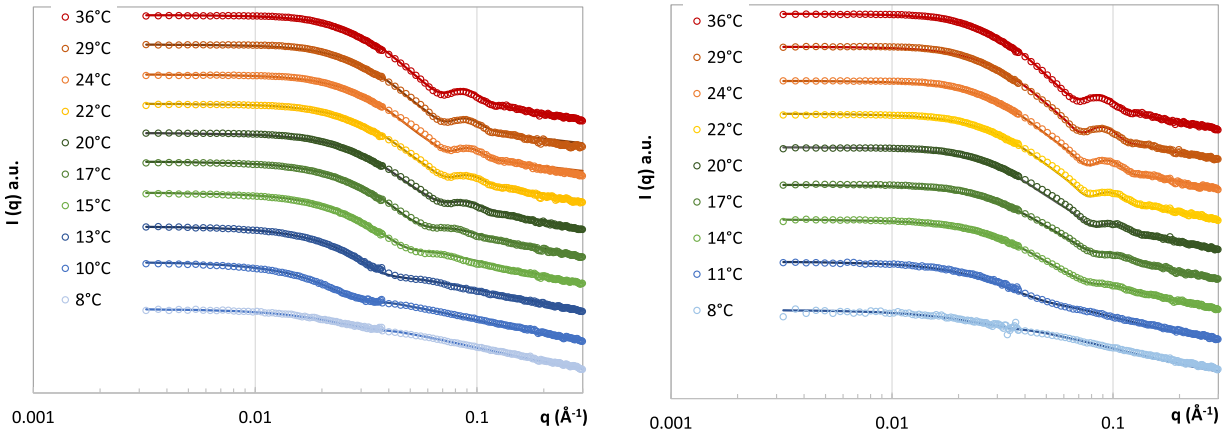

Figure 4. Φ_{F127} = 1%; Φ_{oil} = 0.2% (linalool). Evolution of the SANS scattering intensity as a function of temperature during the micellization/dissolution process. Left: heating; right: cooling. The symbols are the experimental points, and full lines are the fits. The curves are successively shifted vertically by a factor of 10 in intensity to improve the readability.

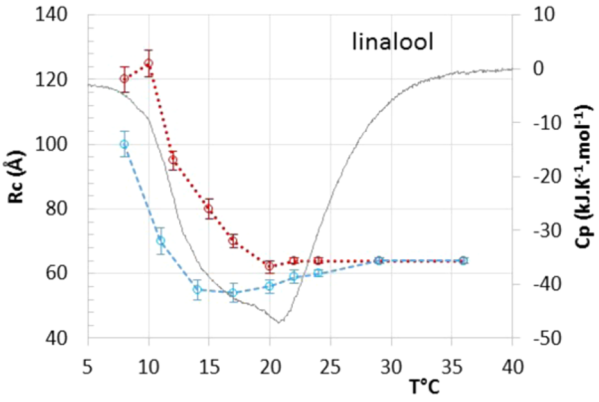

Figure 5. Evolution of the micellar core radius during the heating and cooling micellization/demicellization process for linalool. Left axis: (red) heating phase; (blue) cooling phase. The dotted lines are guides for the eyes. Right axis: corresponding thermogram during the heating phase.

shown for the SANS data. The highly hydrated PEO shell is almost invisible by neutron. On the contrary, by X-ray, the scattering length density of PPO core is close to the scattering length density of water and micelles are in shell contrast. In consequence, the characteristic oscillation of the rather monodisperse sphere appears at 0.1 $Å^{-1}$ value for the SANS data and at a much lower q-value, 0.046 $Å^{-1}$, for the X-ray data. The combined SANS and SAXS analysis in the absolute scale yields to a core radius of 45 Å and a shell thickness of 61 Å.

The fitted scattering length densities of the core are 1.4×10^{10} and 9.55×10^{10} cm^{-2} for neutron and X-ray, respectively. For the neutron analysis, the hydration of the polymer induces an increase of the SLD whereas with X-ray, it corresponds to a decrease compared with the theoretical calculated values (Table 3). This is consistent with a hydration of 17 and 89% (eq 1 and eq 2) of the PPO and PEO parts, respectively, in good agreement with previous studies on different Pluronics.[52,53] The aggregation number (eq 5) is N_{aggr} = 55, and the surface per head group is around 450 $Å^2$ (eq 6).

Oil-Loaded F127 Micelles. An example of SANS and SAXS scattering data for F127 1% loaded with 0.2% linalool at 37 °C is shown in Figure 6. Compared with the F127 in D_2O, one observes a shift of the oscillations toward low q, due to the swelling, and especially for X-ray, the amplitude of the first oscillation is enhanced and a second smaller oscillation is visible. In a first approach, the data analysis is performed assuming a core−shell model where the core is a homogeneous mixture of PPO, oil, and water and the shell contains PEO and water. The data fitting is shown as a continuous line in Figure 6.

The radius of the core is 63 Å, corresponding to an increase of 18 Å compared to that of the F127 micelles alone. The shell thickness decreases slightly to 58 Å. The average SLD of the core decreases to 1.2×10^{10} and 9.4×10^{10} cm^{-2} for neutron and X-ray, respectively, in agreement with the fact that linalool has lower SLD both for neutron and X-ray. The shell SLD is unchanged. The linalool is then incorporated in the hydrophobic part of the micelle. However, if the

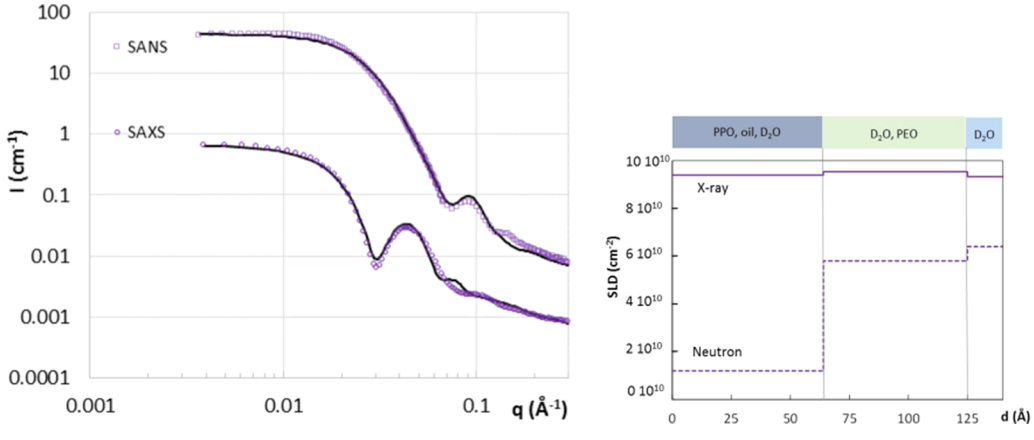

Figure 6. (Left) SANS and SAXS scattering data for Φ_{F127} = 1% and $\Phi_{linalool}$ = 0.2% at 37 °C. The full lines are the calculations considering a core−shell model. (Right) scattering length profiles for SANS and SAXS experiment.

DOI: 10.1021/acs.langmuir.8b03050
Langmuir 2018, 34, 13395−13408

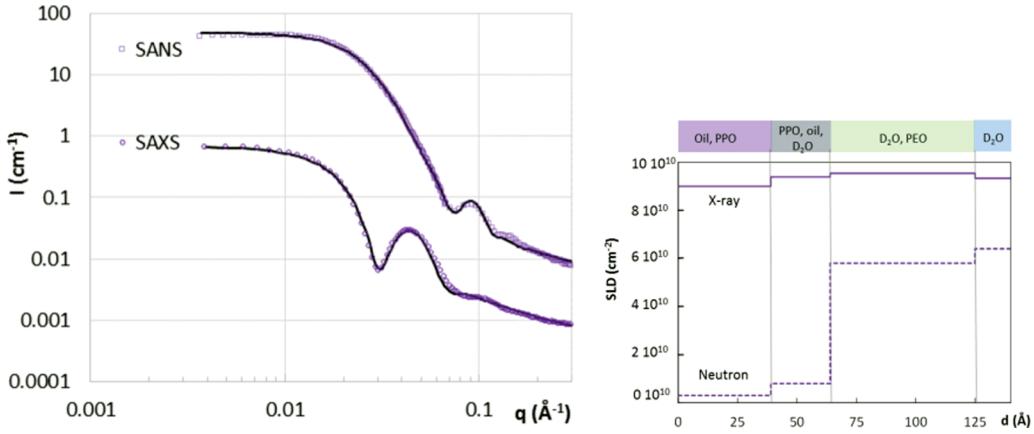

Figure 7. (Left) SANS and SAXS scattering data for Φ_{F127} = 1% and $\Phi_{linalool}$ = 0.2% at 37 °C. The full lines are the calculation considering a core−two-shell model. (Right) scattering length profiles for SANS and SAXS experiments.

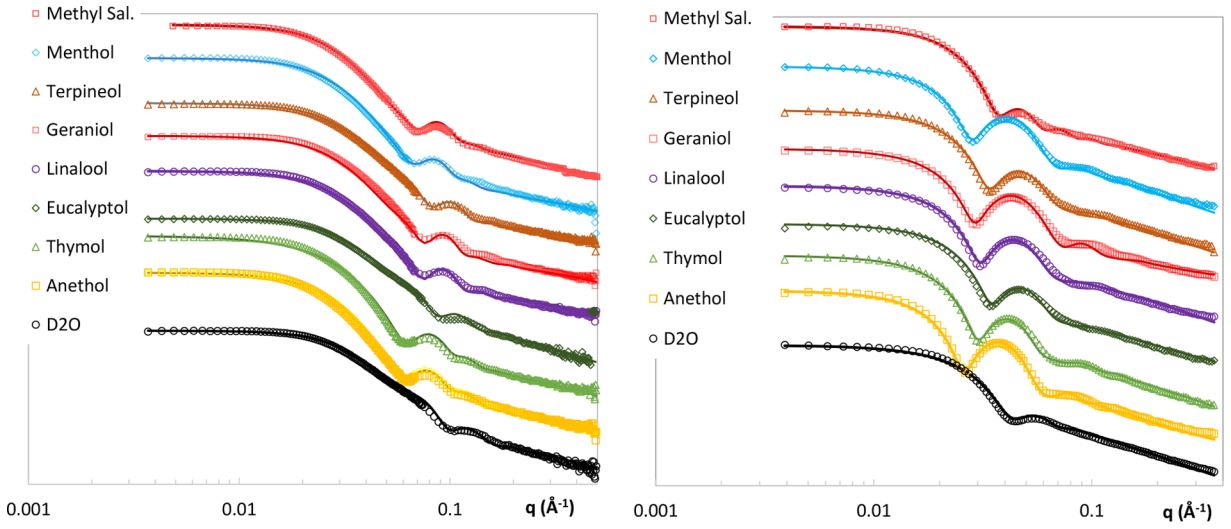

Figure 8. F127 loaded with the synthetic molecules. Φ_{F127} = 1% and Φ_{oil} = 0.2%. SANS (left) and SAXS (right). Symbols are the experimental data; full lines are the best fits obtained with the core-two-shell model. The curves are shifted in intensity by a factor of 10 for better readability.

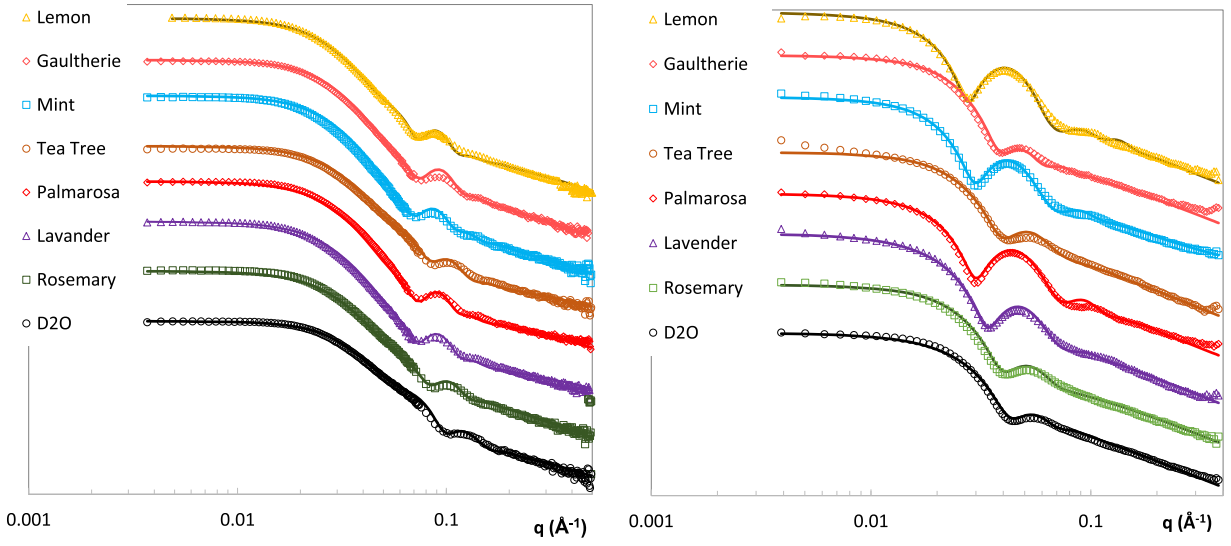

Figure 9. F127 loaded with the essential oils. Φ_{F127} = 1% and Φ_{oil} = 0.2%. SANS (left) and SAXS (right). Symbols are the experimental points; full lines are the calculations obtained with the core−two-shell model. The curves are shifted in intensity by a factor of 10 for better readability.

DOI: 10.1021/acs.langmuir.8b03050
Langmuir 2018, 34, 13395−13408

core−shell model fits in a satisfactory way the first oscillation, we observe a systematic discrepancy between experimental data and the model for the second and smaller oscillation. The data analysis can be improved by considering a core−two-shell model, and the fitting results with the corresponding SLD profiles are shown in Figure 7. We find a first core radius R_0 of 33 Å with an SLD of 0.7 × 10^{10} cm^{-2} (neutron) and 8.95 × 10^{10} cm^{-2} (X-ray) in between the SLD of the pure oil and PO group. The second layer has a thickness of 30 Å with an SLD of 1.3 × 10^{10} cm^{-2} (neutron) and 9.47 × 10^{10} cm^{-2} (X-ray). In total, the radius of the hydrophobic core $R_0 + e_{PPO}$ is still equal to 63 Å, as found with the simple core−shell model. The third layer has a thickness of 58 Å, with SLDs of 5.55 × 10^{10} and 9.58 × 10^{10} cm^{-2} for neutron and X-ray, respectively.

In the following, the data analysis is performed using a core−two-shell model. During the fitting procedure, the radius and SLD values are closely interdependent. However, simultaneous SANS and SAXS data analysis combined with constraints on the parameter range permit to improve the reliability on the parameters. The SANS data analysis allows to determine the total radius of the hydrophobic part, whereas the SAXS permits a precise estimation of the total micellar radius and is more sensitive to the differences in scattering length densities, $\Delta\rho$, between the different shells as the contrast is close to zero. With SAXS, a 5% variation of the SLD shifts significantly the position and the amplitude of the second oscillation. By SANS, the relative error on SLD can reach 15%. The total radius of the hydrophobic core ($R_0 + e_{PPO}$) is determined within ±2 Å accuracy but the individual error on R_0 and e_{PPO} is of the order of ±4 Å.

Figures 8 and 9 present the SANS and SAXS results for the synthetic molecules and EOs, respectively. The data are shifted by a factor of 10 in intensity for a better readability. The sample with limonene has not been measured by SAXS, and the SANS data is shown in Figure S13 in the Supporting Information. Tables 5−7 summarize the different parameters extracted from the data analysis.

We first focus on the synthetic molecules. The parameters (core radius, shell thickness, and volume fraction) obtained from the combined SANS and X-ray data analysis are perfectly consistent. For a constant 0.2% added oil concentration, the swelling of the micelles depends on the nature of the additive. It varies between 6 Å for the less swollen micelles with eucalyptol to 29 Å for the larger micelles with anethol or thymol. We can note that the core diameter remains smaller than the extended length of the PPO block (around 300 Å taking 4.6 Å for the monomer length[20]). The aggregation number (eq 5) increases from 55 for the F127 alone to 160 for the largest micelles, and correspondingly, the density number of micelles decreases by a factor 3. For eucalyptol and limonene, a significant decrease of the surface per head group is found. With the other molecules, it remains relatively constant and close to the reference value of the F127 micelles in D_2O.

It is important at this step to confirm the consistency between the parameters extracted from the data fitting and the sample composition (known from the preparation) and thus to establish a material balance equation.

The oils have a given solubility in water, which is not negligible in the case of eucalyptol and linalool. As before, for the insertion limit, we suppose that this solubility is not modified by the presence of the Pluronic micelles. In the monophasic domain, the excess oil volume fraction that is not soluble in water and participates in the micelle swelling is equal to

$$\Phi^{e}_{oil} = \Phi_{oil} - (S_{oil}/d_{oil})/1000 \quad (8)$$

where S_{oil} and d_{oil} are the oil−water solubility in g/L and the density, respectively.

The PPO volume fraction represents 33% of the molecular volume of an F127 chain. From the data fitting of the pure Pluronic micelles, we have determined that the hydrophobic core contains also a volume fraction f_c of D_2O. For the numerical calculation, f_c is fixed at 0.1, a value slightly smaller than that for the F127 alone, to be consistent with the increase of enthalpy measured by DSC. The total volume of the hydrophobic part that forms the micelles is

Table 5. F127 1% Solution Loaded with 0.2% Synthetic Molecules: SANS and SAXS Data Parameters Issued from the Calculation with a Core−Two-Shell Model

	D_2O	anethol	thymol	eucalyptol	linalool	geraniol	terpineol	menthol	methyl salicylate	limonene
Φ_m	0.047	0.035	0.035	0.038	0.035	0.042	0.044	0.035	0.040	0.033
R_0 (Å) (±4 Å)		44	44	51	33	34	27	41	66	33
e_1 (Å) (±4 Å)	45	30	30		30	30	30	30		30
e_s (Å) (±2 Å)	61	61	60	60	58	61	61	61	60	64
ρ_0 (cm^{-2}) SANS		1.10×10^{10}	0.95×10^{10}	1.10×10^{10}	0.7×10^{10}	0.4×10^{10}	0.5×10^{10}	0.3×10^{10}	1.48×10^{10}	0.4×10^{10}
ρ_1 (cm^{-2}) SANS	1.4×10^{10}	1.30×10^{10}	1.34×10^{10}		1.30×10^{10}	1.30×10^{10}	1.30×10^{10}	1.35×10^{10}		1.4×10^{10}
ρ_s (cm^{-2}) SANS	5.80×10^{10}	5.60×10^{10}	5.60×10^{10}	5.75×10^{10}	5.55×10^{10}	5.80×10^{10}	5.70×10^{10}	5.60×10^{10}	5.65×10^{10}	5.70×10^{10}
ρ_0 (cm^{-2}) SAXS		9.17×10^{10}	9.23×10^{10}	9.36×10^{10}	8.95×10^{10}	8.80×10^{10}	8.95×10^{10}	8.90×10^{10}	9.68×10^{10}	
ρ_1 (cm^{-2}) SAXS	9.55×10^{10}	9.54×10^{10}	9.54×10^{10}		9.47×10^{10}	9.43×10^{10}	9.54×10^{10}	9.54×10^{10}		
ρ_s (cm^{-2}) SAXS	9.54×10^{10}	9.58×10^{10}	9.58×10^{10}	9.58×10^{10}	9.58×10^{10}	9.56×10^{10}	9.56×10^{10}	9.59×10^{10}	9.90×10^{10}	
Φ^{e}_{oil}		0.19	0.11		0.01	0.19	0.16	0.15	0.16	0.20
R^{tot}_{oil} (Å) (±2 Å)	45	74	74	51	63	64	57	71	66	63
R_{tot} (Å) (±2 Å)	106	139	133	111	121	125	118	132	126	127
N_p (cm^{-3})	9.42×10^{15}	3.40×10^{15}	3.47×10^{15}	6.46×10^{15}	4.72×10^{15}	5.13×10^{15}	6.39×10^{15}	3.63×10^{15}	4.77×10^{15}	3.85×10^{15}
N_{agg}	56	160	155	84	114	105	85	149	113	140
σ (Å^2)	447	432	442	390	435	488	483	423	483	355
$R^{calc}_{hyd.}$ (Å)	47	73	69		58	64	58	70	63	70

DOI: 10.1021/acs.langmuir.8b03050
Langmuir 2018, 34, 13395−13408

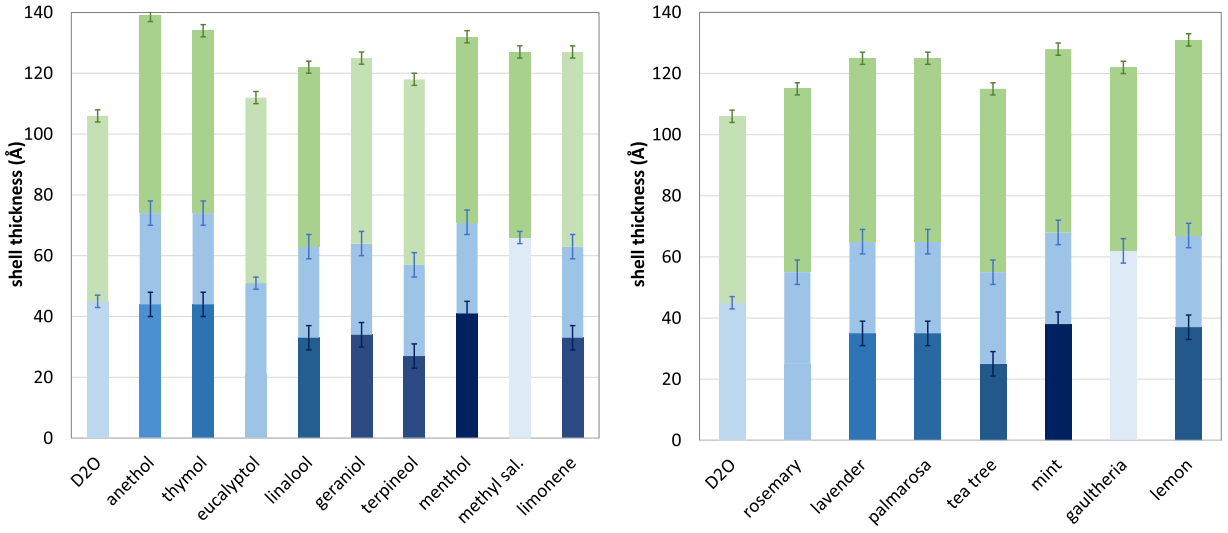

Figure 10. Φ_{F127} = 1% and Φ_{oil} = 0.2% at 37 °C. Summary of the sizes of the different shells. (Blue) hydrophobic core; (green) PEO shell. The darker the color, the lower the SLD. (Left) molecules. (Right) essential oils.

Table 6. F127 1% Solution Loaded with 0.2% of Essential Oils: SANS Data Parameters Issued from the Calculation with a Core−Two-Shell Model

	D_2O	lemon	rosemary	lavender	palmarosa	tea tree	mint	gaultheria
Φ_m	0.047	0.033	0.038	0.035	0.036	0.037	0.037	0.04
R_0 (Å) (±4 Å)		46	55	36	34	25	38	32
e_1 (Å) (±4 Å)	45	19		30	30	30	30	30
e_s (Å) (±2 Å)	61	68	61	60	60	60	60	60
ρ_0 (cm^{-2})		0.4×10^{10}	1.1×10^{10}	0.4×10^{10}	0.17×10^{10}	0.18×10^{10}	0.8×10^{10}	1.3×10^{10}
ρ_1 (cm^{-2})	1.4×10^{10}	1.4×10^{10}		1.2×10^{10}	1.0×10^{10}	1.0×10^{10}	1.4×10^{10}	1.6×10^{10}
ρ_s (cm^{-2})	5.75×10^{10}	5.6×10^{10}	5.6×10^{10}	5.6×10^{10}	5.6×10^{10}	5.6×10^{10}	5.6×10^{10}	5.6×10^{10}
N_p (cm^{-3})	9.42×10^{15}	3.35×10^{15}	5.81×10^{15}	4.18×10^{15}	4.51×10^{15}	5.81×10^{15}	4.2×10^{15}	5.26×10^{15}
N_{agg}	56	160	92	128	119	92	127	182
σ ($Å^2$)	447	331	412	426	432	411	456	473

Table 7. SAXS Data Parameters for the F127 1% Solution Loaded with 0.2% of Essential Oils: SAX Data Parameters Issue from the Calculation with a Core−Two-Shell Model

	D_2O	lemon	rosemary	lavender	palmarosa	tea tree	mint	gaultheria
Φ_m	0.047	0.033	0.033	0.033	0.032	0.033	0.037	0.035
R_0 (Å) (±4 Å)		46	45	26	34	45	38	28
e_1 (Å) (±4 Å)	45	19		30	30		30	60
e_s (Å) (±2 Å)	61	68	61	61	61	61	61	61
ρ_0 (cm^{-2})		8.95×10^{10}	9.45×10^{10}	9.0×10^{10}	8.7×10^{10}	9.44×10^{10}	8.9×10^{10}	9.6×10^{10}
ρ_1 (cm^{-2})	9.45×10^{10}	9.45×10^{10}		9.45×10^{10}	9.39×10^{10}		9.45×10^{10}	9.55×10^{10}
ρ_s (cm^{-2})	9.54×10^{10}	9.54×10^{10}	9.55×10^{10}	9.55×10^{10}	9.54×10^{10}	9.54×10^{10}	9.54×10^{10}	9.54×10^{10}

$$\Phi_{hyd.} = \frac{\Phi_{F127} \times 0.33}{(1 - f_c)} + \Phi_{oil}^{e} \quad (9)$$

Φ_{F127} is the volume fraction of F127. The CMC being of the order of 10^{-5} mol/L (0.01%), the concentration of free monomers in solution is negligible.

The volume of the hydrophobic part per micelle is obtained by dividing the total hydrophobic volume by the density number of micelles obtained from data fitting. The core radius is obtained following

$$V_{hyd.} = \Phi_{hyd.}/N_p \text{ and } R_{hyd.}^{calc} = \sqrt[3]{\frac{3}{4\pi}\Phi_{hyd.}} \quad (10)$$

Φ_{oil}^{e} and $R_{hyd.}^{calc}$ are gathered in Table 5. The calculated hydrophobic radii are in perfect agreement (within 1 Å) with the experimental values for anethol, geraniol, 4-terpineol, and menthol. Eucalyptol, linalool, and methyl salicylate, which have the highest water solubility, swell more than expected. With solubility in water of 3 g/L, a 0.2% eucalyptol volume fraction is in principle below the water solubility limit and it could be expected that the oil remains in water. However, a small swelling of 6 Å is observed, indicating that part of the oil enters into the micellar core. Similarly, linalool, with a remaining water insoluble oil fraction of 0.01% swells significantly. Such a situation where it is more favorable for the oil to be located inside the micelles even at concentrations where it is soluble in the aqueous solution was already observed with benzyl alcohol in P85 micelles.[54]

Inversely, limonene has a smaller experimental swelling. From the phase diagram (Figure S1), it is known that the concentration (0.2%) of limonene is above the solubility limit, found at 0.09%. If one considers this latter concentration as the incorporated volume in the micelles, the predicted radius $R_{hyd.}^{calc}$ is 65 Å, in good agreement with the experimental value (63 Å).

DOI: 10.1021/acs.langmuir.8b03050
Langmuir 2018, 34, 13395−13408

From the scattering length densities of the different layers, the localization of the oil molecules can be assessed. For eucalyptol and methyl salicylate, the data analysis shows that the oil and the PO groups are homogeneously mixed. For the other molecules, the inner shell has a lower SLD, consistent with an enriched oil-loaded core in which radius R_0 varies between 27 Å for the less swollen micelles with terpineol and up to 45 Å with anethol. The core contains more than 70% of oil. It is surrounded by a second layer with a constant size of 30 ± 4 Å. Compared with the micelle in D_2O alone, the SLD slightly decreases for both SANS and SAXS, indicating the presence of small amounts of oil (between 5 and 10%). Finally, the hydrophilic shell is unchanged. For anethol and limonene only, the shell thickness increases are of 5 Å. The slight decrease of SLD with SANS and the increase with SAXS is consistent with a small dehydration of the EO groups (ca. 87% instead of 89%), rather than the presence of oil molecules, which would have also reduced the SLD value.

It is now relevant to compare these results with the behavior of the essential oils (Figure 10 (right) and Tables 6 and 7). In this case, we observe a significant discrepancy between the SANS and SAXS parameter sizes, especially with rosemary, tea tree, and to a smaller extent gaultheria. The deswelling observed by SAXS can be explained due to sample ageing (SANS and SAXS experiments were performed with a time lapse of 2 weeks) and decrease of oil concentration due to strong volatility.

However, focusing mainly on the SANS results, the swelling trends observed with the essential oils match the results obtained with the main molecule that composes the oil. Lavender, palmarosa, mint, and lemon induce the largest swellings. Rosemary and tea tree are the less swelling oils. However, the measured swellings are often below the expected values $R_{hyd.}^{calc}$. It must be recalled that essential oils are blends of a large variety of molecules with different solubilities, which is not considered in the applied model.

DISCUSSION

What are the relevant parameters that govern the insertion of oil in micelles and more specifically in Pluronic micelles?

The solubilization of hydrophobic molecules in surfactant and Pluronic micelles has been intensively investigated, and Nagarajan et al. have developed a predictive thermodynamic model to calculate the swelling and the aggregation number of micelles in presence of additives.[30−34] In this model, the interactions at the water−micelle interface control the surface per micelle and the volume, and they further determine the final volume available for the oil in the core. Larger oil molecules enter to a lesser extent in micelles. To explain difference of solubilization for molecules with similar volumes, the interfacial tension γ_{ow} between the oil and the water can be considered. Molecules with the lowest interfacial tensions have enhanced solubilization. The solubilization in block copolymer (Pluronic) micelles is, however, more delicate. In addition to a specific preferred interfacial area, the configurational degree of freedom of the (long) hydrophobic chains in the core has to be maximized and the interaction between the core block and the solute must be considered. In the Naragajan and Ganesh[31] model, the oil is considered to have a uniform concentration in the core region. The change of the chemical potential due to the aggregation in presence of oil is the sum of several free-energy contributions, and among them two depend on the nature of the solute (oil), the others being linked to the copolymer nature. In the first oil-dependent term, the energy arising from the mixture of the oil with the PO unit is quantified within the framework of the Flory theory[55] where the Flory−Higgins parameter is calculated from the Hildebrand solubility parameters. As the magnitude of the Flory parameter decreases, the oil-loading capability is supposed to increase. The second term related to the nature of the oil considers the water−oil interface tension. When the oil−water interface tension is low, the oil incorporates more easily at the interface, the surface per head group at the interface increases, and the aggregation number decreases.

To compare the model expectation with the experimental results, complementary oil−water (D_2O) interfacial tensions γ_{ow} have been performed using the drop shape analysis method (Table S1). The oils have relatively low water interfacial tensions comprised between 10 and 20 mN/m. We note here that the γ_{ow} values obtained for limonene and lemon essential oil were reproducibly significantly lower (16 mN/m) than values reported in the literature (∼40 mN/m).[56,57]

The Flory parameters $\chi_{o\text{-}PPO}$ were calculated from the Hansen parameters. The Hansen parameters were not found for 4-terpineol but were found for α-terpineol whose structure differs with the −OH position. This has a major consequence on the water solubility and consequently certainly also on the Hansen parameters.

Table S1 compares $\chi_{o\text{-}PPO}$ and γ_{ow} with (1) the solubility limits and (2) the hydrodynamic radius at the insertion limit. Unfortunately, it is not possible to extract any systematic trend between these different parameters. It is worth noticing that contrary to the Nagarajan model that assumes a homogeneous mixture between oil and PPO, the scattering experiments have clearly evidenced a partial phase separation between the oil and the PPO.

It is finally important to put back these results in the context of the literature that also includes ionic surfactants. In ref 16, the incorporation of 15 perfume molecules in SDS micelles was investigated. The location of the oil in the micelle, as identified by SAXS and NOESY experiments, was discussed as a function of the log(P) value. Hydrophilic perfumes with log(P) < 2.0 are incorporated at a level of 80−85% into the SDS micelles (many free perfume molecules are left in the bulk solution but less than the solubility limit without surfactant) and locate in the head group regions. They almost do not change the size of the micelles. Very hydrophobic perfumes with log(P) above 3.5, such as limonene, are fully solubilized in the SDS micelles and locate in the core of micelles, causing significant swelling of the micelle (the compositions investigated correspond to approximately 0.25 oil molecules per SDS molecule). In the intermediate log(P) range (2.0−3.5), the micellar size and the aggregation number increase but to a lesser extent than that in the range of log(P) above 3.5. The results are attributed to the influence of other molecular structure factors besides the degree of hydrophilicity/hydrophobicity. The previous results are confirmed in ref 17 in which the effects of eight fragrance molecules in the ternary phase diagram water/C12E8/perfume were investigated. In particular, it is considered that the variation of the hydrophilic−lipophilic balance (HLB) temperature at which the system has a zero curvature is directly linked to the location of the perfume molecule in the aggregates. From SAXS measurements, it is found that perfume compounds, which reduce the HLB temperature greatly, tend to penetrate into the surfactant palisade layer, are intercalated with the surfactant chains, and increase the cross-sectional area of one surfactant. This is the case for molecules with a hydroxyl group at the end and those that act as a lipophilic surfactant or cosurfactant. Inversely, when the perfume compounds are less amphiphilic in character, like hydrocarbons, they tend to be solubilized deep inside the hydrocarbon part of the surfactant, forming a perfume core. Similarly, in 18, the effect of more or less polar additives, such as hexanol, geraniol, and toluene, on

DOI: 10.1021/acs.langmuir.8b03050
Langmuir 2018, 34, 13395−13408

the F108 micellization was investigated. The addition of the alcohols hexanol and geraniol leads to a more pronounced decrease of the CMT than that of the more hydrophobic toluene molecule. This is corroborated by the SANS characterization that shows a pronounced increase of the scattering intensity and thus the growth of the micelles with decrease of the amount of water incorporated initially in the micellar cores. These findings, concerning both the CMT and the structure perfectly matched the results found here for the F127 micelles. Finally, a last example concerns the incorporation and location of fragrances with different polarities in lamellar P104 phases.[29] Phenethyl alcohol increases the interfacial area and is mainly located at the PEO/PPO interface. Benzaldehyde increases the interfacial area but to a lesser extent, and a part of it contributes to the interface whereas the other is located inside the polar/apolar domain. For limonene, the interfacial area is kept almost constant and is located deep inside the apolar part.

SUMMARY AND CONCLUSIONS

The combination of DSC, SANS, and SAXS experiments allowed achieving a detailed picture of the structure of Pluronic F127 micelles loaded with different essential oils and the synthetic pure molecules. The principal characteristics of the loaded micelle are gathered in Table S2. We observed that the insertion limit varied with the nature of the oil and the F127 could solubilize between 8% (limonene) up to 40% (4-terpineol) of its own volume. The addition of oil induced major changes of the micellar characteristics. First, the oil molecules favored the micellization and decreased the CMT. Thymol had the stronger effect, lowering the CMT below 0 °C. With linalool and geraniol, the CMT dropped to around 11 °C. The addition of the other molecules showed less influence on the CMT, which was found around 19 °C. For all oils investigated, the increase of the enthalpy of micellization reflected, compared to that of pure F127, an enhanced dehydration of the PO groups. The SANS characterization during micellization process as a function of temperature revealed the presence of large structures well below the CMT, which is not observed for the pure Pluronic systems. Their size was maximal at the CMT, shrinking afterward to the final equilibrium value, which was achieved a few degrees after the maximum of the endothermic peak. The cooling phase revealed a strong hysteresis in the micellar phase, which could be related to the slow relaxation time described by Aniansson and Walls.[50] A quantitative combined SANS and SAXS data analysis was performed at 37 °C, showing that the micelles kept their spherical shape and swelled. Except for eucalyptol and methyl salicylic, which are homogeneously distributed in the core, the micelles could be described as an almost purely oily core surrounded by a first shell composed mostly of PPO and less percentage of oil, stabilized in water by the highly hydrated PEO layer that was almost unchanged compared to the micelle without oil in water. The maximal swelling, obtained with anethol corresponds to an increase of 16% of the radius of the micelles. This remains, however, relatively small, and consequently it is more accurate to describe the system as "oil-loaded micelles" rather than "microemulsion".

There is no direct relationship between the decrease of the CMT, the increase of the micellization enthalpy, the swelling of the core, and the location of the oils within the hydrophobic domain. In the case of very hydrophobic molecules, such as limonene, the oil rapidly separates, forming oil droplets and does not enter into the micelles. On the contrary, the most hydrophilic oil remains in the water phase. In these extreme cases, the swelling and loading of the Pluronic micelles is low. In the intermediate domain, the oil solubilization and localization in F127 micelles result from a complex interplay between polarity, water solubility, water interfacial tension, and molecular architecture, which allow for accommodating such large molecules in long PPO chains.

ASSOCIATED CONTENT

Supporting Information

The Supporting Information is available free of charge on the ACS Publications website at DOI: 10.1021/acs.langmuir.8b03050.

SANS and SAXS data analysis: models used to analyze the experimental data; solubilization limit of the oils in the pluronic micelles: maximal total volume of oil before the appearance of oil droplets; evolution of the scattering intensity as a function of temperature during the micellization or demicellization processes for linalool, anethol, geraniol, eucalyptol, menthol, methyl salicylate, and thymol; summary of the evolution of the size of the aggregates with temperature for the different oil molecules compared with DSC thermograms; complementary SANS and SAXS data analysis at 37 °C: detailed analysis of the pure pluronic micelles; SANS scattering curves of F127 1% and limonene 0.2%; Hansen and Flory parameters and interfacial tension for the oil molecules; summary of the characteristic parameters of the 1 vol % F127 oil-loaded micelles (PDF)

AUTHOR INFORMATION

Corresponding Author

*E-mail: grillo@ill.fr.

ORCID

I. Grillo: 0000-0002-5774-6773

S. Prévost: 0000-0002-6008-1987

Notes

The authors declare no competing financial interest.

ACKNOWLEDGMENTS

The authors are very grateful to the ESRF and for the time on D2AM for the preliminary characterizations and for the test time on ID02 giving the results presented in this paper. We thank the ILL for the beam time on the D22 and D33 instruments and the Partnership for Soft Condensed Matter (PSCM) for the complementary measurements (DSC and drop shape analysis). The neutron data set is available at http://doi.ill.fr/10.5291/ILL-DATA.9-10-1422.[58] We would like to thank Prof. T. Zemb (ICSM, France) for fruitful advice on micellization process, Dr. J. Combet (ICS, France) for the help during the SANS experiments, and Dr. E. di Cola (ILL, Univ di Milano, Italy) for the careful reading and valuable comments on the manuscript.

REFERENCES

(1) García, M. T.; Gracia, I.; Duque, G.; de Lucas, A.; Rodríguez, J. F. Study of the solubility and stability of polystyrene wastes in a dissolution recycling process. *Waste Manage.* **2009**, *29*, 1814−1818.

DOI: 10.1021/acs.langmuir.8b03050
Langmuir 2018, 34, 13395−13408

(2) Shah, A.; Shahzad, S.; Munir, A.; Nadagouda, M. N.; Khan, G. S.; Shams, D. F.; Dionysiou, D. D.; Rana, U. A. Micelles as Soil and Water Decontamination Agents. *Chem. Rev.* **2016**, *116*, 6042−6074.
(3) Bilia, A. R.; Bergonzi, M. C.; Guccione, C.; Manconi, M.; Fadda, A. M.; Sinico, C. Vesicles and micelles: Two versatile vectors for the delivery of natural products. *J. Drug Delivery Sci. Technol.* **2016**, *32*, 241−255.
(4) El Asbahani, A.; Miladi, K.; Badri, W.; Sala, M.; Addi, E. H. A.; Casabianca, H.; El Mousadik, A.; Hartmann, D.; Jilale, A.; Renaud, F. N. R.; Elaissari, A. Essential oils: From extraction to encapsulation. *Int. J. Pharm.* **2015**, *483*, 220−243.
(5) Majeed, H.; Bian, Y.-Y.; Ali, B.; Jamil, A.; Majeed, U.; Khan, Q. F.; Iqbal, K. J.; Shoemakere, C. F.; Fang, Z. Essential oil encapsulations: uses, procedures, and trends. *RSC Adv.* **2015**, *5*, 58449−58463.
(6) Miyako, Y.; Khalef, N.; Matsuzaki, K.; Pinal, R. Solubility enhancement of hydrophobic compounds by cosolvents: Role of solute hydrophobicity on the solubilization effect. *Int. J. Pharm.* **2010**, *393*, 48−54.
(7) Valero, M.; Castiglione, F.; Mele, A.; da Silva, M. A.; Grillo, I.; González-Gaitano, G.; Dreiss, C. A. Competitive and Synergistic Interactions between Polymer Micelles, Drugs, and Cyclodextrins: The Importance of Drug Solubilization Locus. *Langmuir* **2016**, *32*, 13174−13186.
(8) Causse, J.; Oberdisse, J.; Jestin, J.; Lagerge, S. Small-Angle Neutron Scattering Study of Solubilization of Tributyl Phosphate in Aqueous Solutions of L64 Pluronic Triblock Copolymers. *Langmuir* **2010**, *26*, 15745−15753.
(9) Parekh, P.; Ganguly, R.; Aswal, V. K.; Bahadur, P. Room temperature sphere-to-rod growth of Pluronic P85 micelles induced by salicylic acid. *Soft Matter* **2012**, *8*, 5864−5872.
(10) Ganguly, R.; Kunwar, A.; Kota, S.; Kumar, S.; Aswal, V. K. Micellar structural transitions and therapeutic properties in tea tree oil solubilized Pluronic P123 solution. *Colloids Surf., A* **2018**, *537*, 478−484.
(11) Berthier, D. L.; Schmidt, I.; Fieber, W.; Schatz, C.; Furrer, A.; Wong, K.; Lecommandoux, S. Controlled Release of Volatile Fragrance Molecules from PEO-b-PPO-b-PEO Block Copolymer Micelles in Ethanol-Water Mixtures. *Langmuir* **2010**, *26*, 7953−7961.
(12) Dorman, H. J. D.; Deans, S. G. Antimicrobial agents from plants: antibacterial activity of plant volatile oils. *J. Appl. Microbiol.* **2000**, *88*, 308−316.
(13) Edris, A. E. Pharmaceutical and therapeutic potentials of essential oils and their individual volatile constituents: a review. *Phytother. Res.* **2007**, *21*, 308−323.
(14) Friberg, S. E. Fragrance compounds and amphiphilic association structures. *Adv. Colloid Interface Sci.* **1998**, *75*, 181−214.
(15) Fischer, E.; Fieber, W.; Navarro, C.; Sommer, H.; Benczédi, D.; Velazco, M.; Schönhoff, M. Partitioning and Localization of Fragrances in Surfactant Mixed Micelles. *J. Surfactants Deterg.* **2009**, *12*, 73−84.
(16) Fan, Y.; Tang, H.; Strand, R.; Wang, Y. Modulation of partition and localization of perfume molecules in sodium dodecyl sulfate micelles. *Soft Matter* **2016**, *12*, 219−227.
(17) Kanei, N.; Tamura, Y.; Kunieda, H. Effect of Types of Perfume Compounds on the Hydrophile−Lipophile Balance Temperature. *J. Colloid Interface Sci.* **1999**, *218*, 13−22.
(18) Adams, M.; Lavasanifar, A.; Kwon, G. Amphiphilic block copolymers for drug delivery. *J. Pharm. Sci.* **2003**, *92*, 1343−1355.
(19) Dumortier, G.; Grossiord, J.-L.; Agnely, F.; Chaumeil, J.-C. A Review of Poloxamer 407 Pharmaceutical and Pharmacological Characteristics. *Pharm. Res.* **2006**, *23*, 2709−2728.
(20) Lettow, J. S.; Lancaster, T. M.; Glinka, C. J.; Ying, J. Y. Small-angle neutron scattering and theoretical investigation of poly(ethylene oxide)-poly(propylene oxide)-poly(ethylene oxide) stabilized oil-in-water microemulsions. *Langmuir* **2005**, *21*, 5738−5746.
(21) Guo, L.; Colby, R. H.; Thiyagarajan, P. Temperature and hydrophobic alcohol-induced structural changes of Pluronics micelles. *Phys. B* **2006**, *385−386*, 685−687.
(22) Sharma, P. K.; Reilly, M. J.; Jones, D. N.; Robinson, P. M.; Bhatia, S. R. The effect of pharmaceuticals on the nanoscale structure of PEO-PPO-PEO micelles. *Colloid Surf., B* **2008**, *61*, 53−60.
(23) Causse, J.; Oberdisse, J.; Jestin, J.; Lagerge, S. Small-Angle Neutron Scattering Study of Solubilization of Tributyl Phosphate in Aqueous Solutions of L64 Pluronic Triblock Copolymers. *Langmuir* **2010**, *26*, 15745−15753.
(24) Alexander, S.; Cosgrove, T.; Castle, T.; Grillo, I.; Prescott, S. Effect of temperature, cosolvent and added drug on Pluronic-Flurbiprofen micellization. *J. Phys. Chem. B* **2012**, *116*, 11545−11551.
(25) Liu, H.-Y.; Prévost, S.; Gradzielski, M. Solubilisation of Oils of Different Polarity in Aqueous Solutions of Pluronic Triblock Copolymers. *Z. Phys. Chem.* **2012**, *226*, 675−694.
(26) Patel, V.; Dey, J.; Ganguly, R.; Kumar, S.; Nath, S.; Aswal, V. K.; Bahadur, P. Solubilization of hydrophobic alcohols in aqueous Pluronic solutions: investigating the role of dehydration of the micellar core in tuning the restructuring and growth of Pluronic micelles. *Soft Matter* **2013**, *9*, 7583−7591.
(27) Chat, O. A.; Nazir, N.; Bhat, P. A.; Hassan, P. A.; Aswal, V. K.; Dar, A. A. Aggregation and Rheological Behavior of the Lavender Oil−Pluronic P123 Microemulsions in Water−Ethanol Mixed Solvents. *Langmuir* **2018**, *34*, 1010−1019.
(28) Kim, T.-H.; Han, Y.-S.; Jang, J.-D.; Seong, B.-S. SANS study on self-assembled structures of Pluronic F127 triblock copolymer induced by additives and temperature. *J. Appl. Crystallogr.* **2014**, *47*, 53−59.
(29) Kayali, I.; Khan, A.; Lindman, B. Solubilization and location of phenethylalcohol, benzaldehyde, and limonene in lamellar liquid crystal formed with block copolymer and water. *J. Colloid Interface Sci.* **2006**, *297*, 792−796.
(30) Nagarajan, R.; Barry, M.; Ruckenstein, E. Unusual Selectivity in Solubilization by Block Copolymer Micelles. *Langmuir* **1986**, *2*, 210−215.
(31) Nagarajan, R.; Ganesh, K. Block Copolymer Self-Assembly in Selective Solvents: Theory of Solubilization in Spherical Micelles. *Macromolecules* **1989**, *22*, 4312−4325.
(32) Nagarajan, R. Solubilization in aqueous solutions of amphiphiles. *Curr. Opin. Colloid Interface Sci.* **1996**, *1*, 391−401.
(33) Nagarajan, R. Solubilization of hydrocarbons and resulting aggregate shape transitions in aqueous solutions of Pluronic (PEO−PPO−PEO) block copolymers. *Colloids Surf., B* **1999**, *16*, 55−72.
(34) Nagarajan, R. Solubilization of "Guest" molecules into polymeric aggregates. *Polym. Adv. Technol.* **2001**, *12*, 23−43.
(35) Burt, S. Essential oils: their antibacterial properties and potential applications in foods—a review. *Int. J. Food Microbiol.* **2004**, *94*, 223−253.
(36) Lins, R. F.; Lustri, W. R.; Minharro, S.; Alonso, A.; de Sousa Neto, D. On the formation, physicochemical properties and antibacterial activity of colloidal systems containing tea tree (*Melaleuca alternifolia*) oil Renata. *Colloids Surf., A* **2016**, *497*, 271−279.
(37) Juergens, U. R.; Engelen, T.; Racké, K.; Stöber, M.; Gillissen, A.; Vetter, H. Inhibitory activity of 1,8-cineol (eucalyptol) on cytokine production in cultured human lymphocytes and monocytes. *Pulm. Pharmacol. Ther.* **2004**, *17*, 281−287.
(38) Lucia, A.; Toloza, A. C.; Guzman, E.; Ortega, F.; Rubio, R. G. Novel polymeric micelles for insect pest control: encapsulation of essential oil monoterpenes inside a triblock copolymer shell for head lice control. *Peer J.* **2017**, *5*, No. e3171.
(39) Proudfoot, C. J.; Garry, E. M.; Cottrell, D. F.; Rosie, R.; Anderson, H.; Robertson, D. C.; Fleetwood-Walker, S. M.; Mitchell, R. Analgesia mediated by the TRPM8 cold receptor in chronic neuropathic pain. *Curr. Biol.* **2006**, *16*, 1591−1605.
(40) Wanka, G.; Hoffmann, H.; Ulbricht, W. Phase diagrams and aggregation behavior of poly(oxyethylene)-poly(oxypropylene)-poly(oxyethylene) triblock copolymers in aqueous solutions. *Macromolecules* **1994**, *27*, 4145−4159.

DOI: 10.1021/acs.langmuir.8b03050
Langmuir 2018, 34, 13395−13408

(41) Di Cola, E.; Grillo, I.; Ristori, S. Small Angle X-ray and Neutron Scattering: Powerful Tools for Studying the Structure of Drug-Loaded Liposomes. *Pharmaceutics* **2016**, *8*, 10.
(42) Hecht, E.; Hoffmann, H. Kinetic and calorimetric investigations on micelle formation of block copolymers of the poloxamer type. *Colloids Surf., A* **1995**, *96*, 181−197.
(43) Lam, Y.-M.; Goldbeck-Wood, G. Mesoscale simulation of block copolymers in aqueous solution: parametrisation, micelle growth kinetics and the effect of temperature and concentration morphology. *Polymer* **2003**, *44*, 3593−3605.
(44) Sommer, C.; Pedersen, J. S.; Stein, P. C. Apparent Specific Volume Measurements of Poly(ethylene oxide), Poly(butylene oxide), Poly(propylene oxide), and Octadecyl Chains in the Micellar State as a Function of Temperature. *J. Phys. Chem. B* **2004**, *108*, 6242−6249.
(45) Alexandridis, P.; Hatton, T. A. Poly(ethylene oxide)-poly-(propylene oxide)-poly(ethylene oxide) block copolymer surfactants in aqueous solutions and at interfaces: thermodynamics, structure, dynamics, and modeling. *Colloids Surf., A* **1995**, *96*, 1−46.
(46) Bohorquez, M.; Koch, C.; Trygstad, T.; Pandit, N. A Study of the Temperature-Dependent Micellization of Pluronic F127. *J. Colloid Interface Sci.* **1999**, *216*, 34−40.
(47) Ma, J.-H.; Wang, Y.; Guo, C.; Liu, H.-Z.; Tang, Y.-L.; Bahadur, P. Oil-Induced Aggregation of Block Copolymer in Aqueous Solution. *J. Phys. Chem. B* **2007**, *111*, 11140−11148.
(48) Bharatiya, B.; Guo, C.; Ma, J. H.; Hassan, P. A.; Bahadur, P. Aggregation and clouding behavior of aqueous solution of EO−PO block copolymer in presence of n-alkanols. *Eur. Polym. J.* **2007**, *43*, 1883−1891.
(49) Kastrisianaki-Guyton, E. S.; Chen, L.; Rogers, S. E.; Cosgrove, T.; van Duijneveldt, J. S. Adsorption of F127 onto Single-Walled Carbon Nanotubes Characterized Using Small-Angle Neutron Scattering. *Langmuir* **2015**, *31*, 3262−3268.
(50) Aniansson, E. A. G.; Wall, S. N.; Almgren, M.; Hoffmann, H.; Kielmann, I.; Ulbricht, W.; Zana, R.; Lang, J.; Tondre, C. Theory of the kinetics of micellar equilibria and quantitative interpretation of chemical relaxation studies of micellar solutions of ionic surfactants. *J. Phys. Chem.* **1976**, *80*, 905−922.
(51) Patist, A.; Kanicky, J. R.; Shukla, P. K.; Shahy, D. O. Importance of Micellar Kinetics in Relation to Technological Processes. *J. Colloid Interface Sci.* **2002**, *245*, 1−15.
(52) Pedersen, J. S.; Gerstenberg, M. C. The structure of P85 Pluronic block copolymer micelles determined by small-angle neutron scattering. *Colloids Surf., A* **2003**, *213*, 175−187.
(53) Manet, S.; Lecchi, A.; Impéror-Clerc, M.; Zholobenko, V.; Durand, D.; Oliveira, C.; Pedersen, J. S.; Grillo, I.; Meneau, F.; Rochas, C. J. Structure of Micelles of a Nonionic Block Copolymer Determined by SANS and SAXS. *J. Phys. Chem. B* **2011**, *115*, 11318−11329.
(54) Sharp, M. A.; Washington, C.; Cosgrove, T. Solubilisation of model adjuvants by Pluronic block copolymers. *J. Colloid Interface Sci.* **2010**, *344*, 438−446.
(55) Flory, P. J. *Principle of Polymer Chemistry*; Cornell University Press: Ithaca, NY, 1962.
(56) Arneodo, C.; Baszkin, A.; Benoit, J.-P.; Fellous, R.; Thies, C. Interfacial Studies of Essential Oil-Water Systems. *Colloids Surf.* **1988**, *34*, 159−169.
(57) Pérez-Mosqueda, L. M.; Maldonado-Valderrama, J.; Ramírez, P.; Cabrerizo-Vílchez, M. A.; Muñoz, J. Interfacial characterization of Pluronic PE9400 at biocompatible (air−water and limonene−water) interfaces. *Colloids and Surf., B* **2013**, *111*, 171−178.
(58) Grillo, I.; Combet, J.; Morfin, I. *Insertion of Perfume Molecules in Pluronic Micelles*; Institut Laue-Langevin (ILL), 2015.

DOI: 10.1021/acs.langmuir.8b03050
Langmuir 2018, 34, 13395−13408